Global Biogeochemical Cycles

RESEARCH ARTICLE
10.1029/2019GB006323

Importance of Cadmium Sulfides for Biogeochemical Cycling of Cd and Its Isotopes in Oxygen Deficient Zones—A Case Study of the Angola Basin

D. Guinoiseau[1,2], S. J. G. Galer[1], W. Abouchami[3], M. Frank[4], E. P. Achterberg[4], and G. H. Haug[1]

[1]Climate Geochemistry Department, Max Planck Institute for Chemistry, Mainz, Germany, [2]Now at Institut de Physique du Globe de Paris, Université de Paris, Paris, France, [3]Institut für Geologie und Mineralogie, Universität zu Köln, Cologne, Germany, [4]GEOMAR Helmholtz Center for Ocean Research Kiel, Kiel, Germany

Abstract Understanding oceanic cadmium (Cd) cycling is paramount due to its micronutrient-like behavior in seawater, which has been inferred from its similarity to phosphate (PO_4) cycling. Cadmium concentrations follow a nutrient-like consumption-regeneration cycle in the top of the water column and are mainly controlled by water mass mixing and circulation in the deep ocean. However, an additional scavenging mechanism through cadmium sulfide (CdS) precipitates, occurring within sinking biogenic particles in oxygen deficient zones (ODZ), has been proposed. In this study, we report Cd stable isotope and concentration data for seven vertical seawater profiles sampled during GEOTRACES cruise GA08 in the northern Cape and Angola Basins, which feature a significant ODZ along their eastern margins. Outside the ODZ, Cd cycling is similar to that previously reported for the South Atlantic. While water mass mixing largely controls deep ocean Cd isotope signatures, Cd isotope fractionation in surface waters can be modeled as an open system at steady state buffered by organic ligand complexation. In the ODZ, stronger Cd depletion relative to PO_4 is associated with a shift in δ^{114}Cd toward heavier values, which is indicative of CdS precipitation. Our interpretation is supported by experimental CdS precipitation data and a size-resolved particle model involving bacterial sulfate reduction as a precursor of CdS. Our estimates of the CdS flux to the seafloor (10^7 to 10^9 mol/yr) indicate that CdS precipitation is a significant process of Cd removal and constitutes a nonnegligible Cd sink that needs to be better quantified by Cd isotope analyses of marine sediments.

Key Points:
- Cd cycling in the Angola Basin is overall similar to the rest of the South Atlantic
- Sulfide precipitation exerts control on Cd in Angola Basin oxygen deficient zone
- Flux of CdS to seafloor is important to global oceanic Cd budget

Supporting Information:
- Supporting Information S1

Correspondence to:
D. Guinoiseau,
d.guinoiseau@mpic.de

Citation:
Guinoiseau, D., Galer, S. J. G., Abouchami, W., Frank, M., Achterberg, E. P., & Haug, G. H. (2019). Importance of cadmium sulfides for biogeochemical cycling of Cd and its isotopes in Oxygen Deficient Zones—A case study of the Angola Basin. *Global Biogeochemical Cycles*, *33*, 1746–1763. https://doi org/10.1029/2019GB006323

Received 18 JUN 2019
Accepted 26 NOV 2019
Accepted article online 5 DEC 2019
Published online 17 DEC 2019

1. Introduction

The distribution of dissolved oceanic cadmium (Cd) has been extensively studied over the past 40 years due to its nutrient-like behavior, which mimics that of phosphate (PO_4) in the water column reflecting phytoplankton uptake in the surface ocean and regeneration at depth via sinking particle mineralization (E. A. Boyle et al., 1976; K. W. Bruland, 1980). Our understanding of the oceanic Cd cycle has significantly improved over the past decade based on work in the frame of the international GEOTRACES program (E. Mawji et al., 2015) and analytical development of Cd isotope measurements, which, in addition to Cd concentration data, have provided new insights into the biogeochemical processes controlling its dissolved and particulate distribution (W. Abouchami et al., 2011; W. Abouchami et al., 2014; Conway & John, 2015b; M. Gault-Ringold et al., 2012; E. George et al., 2019; D. J. Janssen et al., 2017; D. J. Janssen et al., 2019; D. J. Janssen et al., 2014; S. G. John et al., 2017; S. Ripperger et al., 2007; M. Sieber et al., 2018; R. C. Xie et al., 2018; R. C. Xie et al., 2019; R. C. Xie et al., 2017; Z. Xue et al., 2013; S. C. Yang, 2015; S.-C. Yang et al., 2018). The existing literature shows that despite the overall similar behaviors of Cd and PO_4, subtle variations with depth in Cd/PO_4 ratios (W. Abouchami et al., 2014; O. Baars et al., 2014; R. Middag et al., 2018) and δ^{114}Cd signatures can be resolved in the water column (e.g. R. C. Xie et al., 2017).

Preferential Cd assimilation by phytoplankton in the surface ocean (J. T. Cullen et al., 1999; H. J. W. de Baar et al., 1994; M. J. Ellwood, 2008; E. S. Lane et al., 2009), differences in remineralization depth of Cd and PO_4 (H. L. Bourne et al., 2018), and/or variable remineralization efficiency of different types of organic particles (D. J. Janssen et al., 2019; Roshan & Wu, 2015; S. Roshan et al., 2017; Wu & Roshan, 2015) have been proposed to account for vertical Cd/PO_4 variabilities. Regarding Cd isotopes, Cd uptake by phytoplankton is accompanied by enrichment in light isotopes in biogenic particles compared to seawater (D. J. Janssen et al., 2019; D. J. Janssen et al., 2014; S.-C. Yang et al., 2018), in line with laboratory culture experiments

(John & Conway, 2014; F. Lacan et al., 2006). Early Cd isotope studies reported heavy surface ocean δ^{114}Cd (up to 5‰) values at picomolar dissolved Cd concentrations that were attributed to closed-system Rayleigh fractionation resulting from biological uptake of light Cd (Conway & John, 2015a, 2015b; S Ripperger et al., 2007). However, recent studies have revealed a homogeneous δ^{114}Cd signature in the ocean surface, particularly in Cd-deficient surface waters from the Atlantic and Pacific Oceans (M. Gault-Ringold et al., 2012; E. George et al., 2019; D. J. Janssen et al., 2017; M. Sieber et al., 2018; R. C. Xie et al., 2018; R. C. Xie et al., 2019; R. C. Xie et al., 2017). These variations have been variably interpreted as reflecting (i) a Cd supply-limited regime (M. Gault-Ringold et al., 2012), (ii) Cd complexation by organic ligands acting to buffer δ^{114}Cd (prevent removal), or alternatively (iii) Cd isotope fractionation in a steady-state open system in surface waters (R. C. Xie et al., 2017).

At depth, the relationship between Cd and PO_4 is "bilinear," with a "kink" at PO_4 concentration of 1.3 μmol/L, the origin of which has been extensively debated (J. T. Cullen, 2006; H. J. W. de Baar et al., 1994; P. Quay et al., 2015). Several recent studies have called upon simple deep-water mass mixing (W. Abouchami et al., 2014; O. Baars et al., 2014; P. Quay et al., 2015; R. C. Xie et al., 2015) with Cd remineralization acting as a secondary controlling factor (R. Middag et al., 2018). A physical control on deep water Cd isotope distribution and its potential use as a conservative water mass tracer was first demonstrated in the Southern Ocean (W. Abouchami et al., 2014) and confirmed by subsequent observations in other oceanic regions (M Sieber et al., 2018; R. C. Xie et al., 2017).

Seawater Cd isotope data in oceanic oxygen deficient zones (ODZs), however, indicate that cadmium sulfide (CdS hereafter) precipitation within sinking biogenic particles may constitute an important mechanism for removal of Cd from the water column (Conway & John, 2015b; D. J. Janssen et al., 2014; R. C. Xie et al., 2019) in agreement with modeling studies (D. Bianchi et al., 2018). The possible occurrence of CdS was first described in the Mauritanian ODZ based on a combination of (1) depletion of dissolved Cd, (2) enrichment of particulate Cd relative to PO_4 and (3) a shift of dissolved δ^{114}Cd toward heavier values (Conway & John, 2015b; D. J. Janssen et al., 2014). The Cd isotope fractionation factor determined experimentally during CdS precipitation in synthetic seawater is $\alpha^{114/110}{}_{\text{Cdsol-CdS}} = 1.00032$ (D. Guinoiseau et al., 2018) and is in agreement with field observations of a seawater Cd isotope shift, as well as with ab initio models (J. Yang et al., 2015). Furthermore, the size-resolved particle model recently developed by Bianchi et al. (2018) predicts that microbial sulfate reduction can occur in coarse particle aggregates (>1 mm) at the upper boundary of ODZs (100–200 m depth), thereby releasing H_2S into solution and thus promoting local CdS precipitation. The model results of Bianchi et al. (2018) agree well with measured Cd and Cd/PO_4 profiles in the particulate phase of the Mauritanian ODZ. Such an active cryptic sulfur cycle has also been proposed in the Chilean (D. E. Canfield et al., 2010), Arabian (B. M. Fuchs et al., 2005), North Pacific (Beman & Carolan, 2013; M. T. Carolan et al., 2015) and Peruvian ODZs (R. C. Xie et al., 2019), based on the identification of sulfide oxidizers and sulfate reducing species in picoplankton and bacterial communities. Nevertheless, the absence of strong Cd depletion or Cd isotope shifts in the North Pacific ODZ (Conway & John, 2015a; D. J. Janssen et al., 2017) indicates that the extent of CdS precipitation may be variable among different oceanic ODZs. The associated particulate δ^{114}Cd data indicate that organic particle mineralization is dominant in the North Pacific ODZ, whereas CdS precipitation, if occurring, was only of minor importance (D. J. Janssen et al., 2019). This is in line with the low particles flux reaching the low-oxygen layer in the North Pacific ODZ compared to that in the Mauritanian ODZ, which might prevent any quantitative CdS precipitation (Conway & John, 2015a). Thus, even if CdS precipitates do indeed form in some oceanic ODZs, the chemical or physical parameters controlling this process still remain uncertain.

The sequestration and export of Cd to marine sediments is mostly associated with burial of particulate non-remineralized organically bound Cd in suboxic ($F_{Cd} = 0.03–2.3.10^7$ mol/yr) and anoxic environments ($F_{Cd} = 0.09–3.6.10^7$ mol/yr) (S. H. Little et al., 2015; Morford & Emerson 1999; Y. Rosenthal et al., 1995; A. van Geen et al., 1995). The effect of sequestration or release of Cd from margin sediments has been discussed in recent Cd isotope studies of the subarctic Pacific and Peru Basin ODZs (D J Janssen et al., 2019; R C Xie et al., 2019). Additionally, the uncertainties of the flux of preserved CdS to the seafloor—with estimates varying from 0.1×10^7 to 1.4×10^9 mol/yr (D. Bianchi et al., 2018; D. J. Janssen et al., 2014)— is mainly a result of a lack of constraint on the stability of CdS complexes as they sink out of ODZs into the oxygenated deep water column.

In this study, we examine the seawater distribution of Cd and its isotopes in the northern Cape Basin and Angola Basin. The eastern margin of these basins features major upwelling systems, and we assess whether CdS precipitation occurs in the well-developed ODZ between 200 and 1,000 m depth. We report seven depth profiles of Cd isotopes and concentrations sampled during GEOTRACES cruise GA08 (Walvis Bay to Walvis Bay, Namibia; 22 November to 27 December 2015). The results show that the Cd isotope characteristics of surface and deep waters, outside the influence of the ODZ, are overall similar to those observed elsewhere in the Southwest Atlantic (R. C. Xie et al., 2017). In particular, our data are consistent with a water mass mixing control at depth and surface Cd isotope fractionation in an open ocean steady-state system buffered by dissolved organic ligands. Importantly, in the top part of the ODZ, the measured Cd depletion associated with a heavier δ^{114}Cd signal is fully consistent with CdS precipitation, in line with previous observations in the Mauritanian or East Tropical South Pacific (ETSP) ODZs (Conway & John, 2015b; S. G. John et al., 2017; R. C. Xie et al., 2019) and the fractionation factor determined experimentally for CdS precipitation (D. Guinoiseau et al., 2018). Altogether, this suggests that CdS precipitation plays a significant role in major ODZs worldwide, with an estimated preserved flux of CdS to the seafloor of 0.87×10^7 to 1.04×10^9 mol/yr, which may thus represent the major pathway of Cd removal from oxygen deficient waters.

2. Materials and Methods

2.1. Hydrography of the Angola Basin

The hydrography of the South Atlantic Ocean, and particularly that of the Angola Basin, has been described in detail in earlier studies (Stramma & England, 1999; Van Bennekom & Berger, 1984). Briefly, the Angola Gyre subsurface circulation is mainly driven by the eastward flowing Equatorial Undercurrent (EUC), South Equatorial Undercurrent (SEUC), and South Equatorial Countercurrent (SECC) (Figure 1). The southward flow out of the Angola Basin is deviated westward by the northwestern branch of the Benguela Current near 20°S forming the Angola-Benguela Front (ABF). Export of water across the ABF of up to 7 Sv (H. U. Lass et al., 2000) is counterbalanced by northward inflow of the Benguela Coastal Current (BCC) reaching latitudes of 10–20°S. This circulation pattern results in the development of an upwelling system centered in the Angola Dome that is characterized by subsurface nutrient-rich waters and hypoxic conditions between 200 and 600 m depth. The influence of the Congo River plume that extends up to 800 km offshore (M. Waeles et al., 2013) is negligible for the sampling area of our study.

Below the surface ocean, low salinity Antarctic Intermediate Water (AAIW), found at depths between 500 and 1,300 m, originates from the Indian Ocean and is advected into the southern Atlantic via the Agulhas Current and is transported further northeastward by the Benguela Current (Suga & Talley, 1995). Between 1,500 and 4,500 m depth, salty and well-oxygenated North Atlantic Deep Water (NADW) enters the Angola Basin through the Romanche Fracture Zone (RFZ) and flows southward (supporting information Figure S2). Antarctic Bottom Water (AABW) contributes to deep ocean waters at depths below 4,000 m and also passes through RFZ on its flow north. A clear distinction between NADW and AABW in the Angola Basin is not possible due to strong vertical mixing that occurs in the RFZ (Stramma & England, 1999). The "unaltered" body of AABW advected from the Southern Ocean characterized by low temperatures and salinity and high nutrient and O_2 concentrations (Figures 1 and S3), as sampled at station TM38 profile (Figure S2), is observed in the northern Cape Basin south of the Walvis Ridge, which acts as a physical barrier to the southward flowing NADW-AABW mixture.

2.2. Sampling and Analytical Methods

Seven vertical profiles and six surface water samples (3 m depth) were collected in the Angola Basin during the GA-08 cruise that took place in the period between 22 November and 27 December 2015 (Figure 2). Sampling of vertical profiles was carried out using a trace metal clean CTD (Conductivity, temperature, depth) sensor (Seabird) and rosette equipped with GO-FLO (Ocean Test Equipment) bottles, whereas surface samples were collected using a towed FISH system. Immediately after collection, the samples were filtered through 0.2 μm Acropack Supor (Pall Corp.) cartridges, transferred into 1 to 10 L high density polyethylene (HDPE, ThermoFisher, Nalgene) bottles and canisters (precleaned in hot acid) and acidified to pH 2 using 12 M ROMIL UpA-grade HCl onboard the ship.

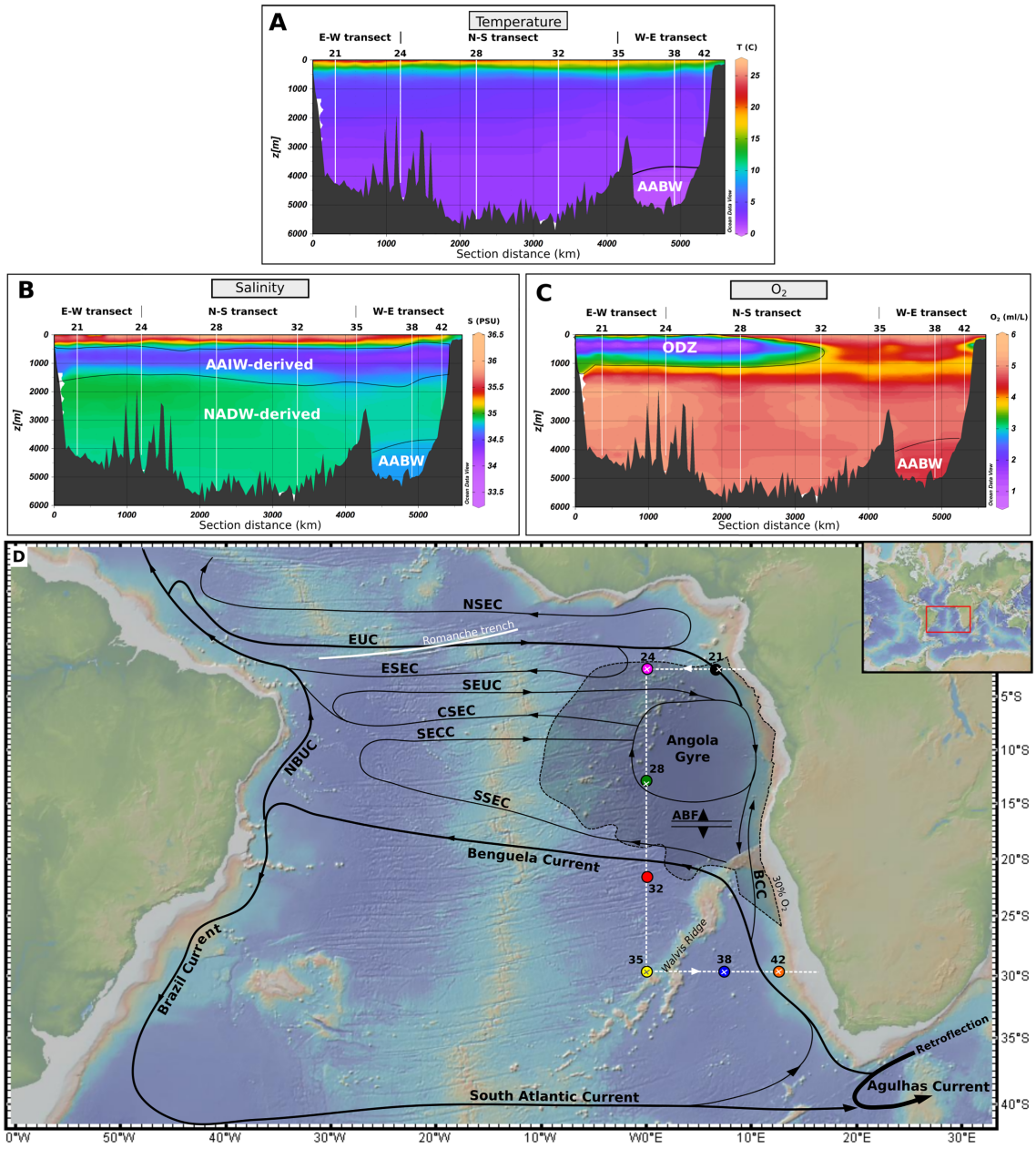

Figure 1. Cross sections of hydrographic parameters along the track of cruise GA08 and schematic subsurface circulation in the South Atlantic Ocean. The section of temperature (a), salinity (b), and O_2 (c) in the three top boxes is represented by the white dashed line on the map (d). In D, the thickness of the black lines is proportional to the volume flow of the currents. The shaded area represents the region where the Angola oxygen deficient zone develops (O_2 concentration below 30% of saturation at 400 m depth). The vertical profiles and TOW-FISH surface samples are displayed as colored dots and crosses, respectively. Acronyms refer to the northern (NSEC), equatorial (ESEC), central (CSEC), and southern (SSEC) branches of the South Equatorial Current (SEC); Equatorial Undercurrent (EUC); South Equatorial Undercurrent (SEUC); South Equatorial Countercurrent (SECC); Benguela Coastal Current (BCC); North Brazil Undercurrent (NBUC). The Angola-Benguela Front (ABF) marks the northern boundary of Benguela Current influence. The schematic circulation pattern is adapted from Stramma and England (1999).

Temperature, salinity and dissolved O_2 were obtained with calibrated Seabird sensors. Unfiltered macronutrient samples (PO_4, NO_3 + NO_2, Si) were collected in acid cleaned polypropylene bottles and analyzed on board by segmented flow injection analysis using a QUAATRO (Seal Analytical) autoanalyzer. The chromatographic separation of Cd was performed in a Class-100 clean laboratory at Max Planck Institute for Chemistry. Briefly, samples were weighed and spiked with a ^{106}Cd-^{108}Cd double spike (see A.-D. Schmitt et al., 2009), equilibrated for 24 hr and separated using two steps as detailed in Abouchami et al. (2011).

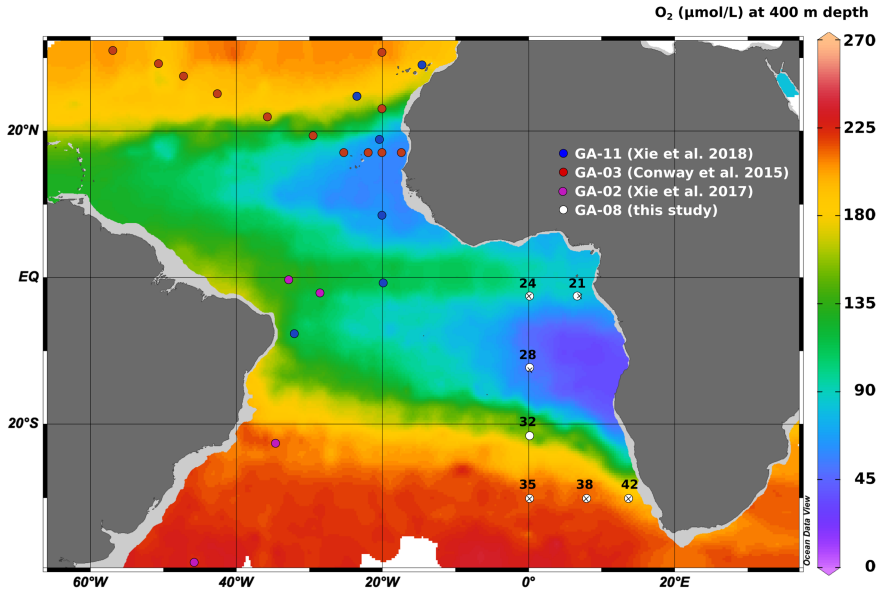

Figure 2. Sampling map of GEOTRACES cruises in the South and tropical Atlantic showing stations for which Cd isotope data are available. The O_2 concentration at 400 m depth is displayed to identify the maximum extent of the Mauritanian and Angola Basin ODZs. Dots refer to vertical profile stations, whereas black crosses denote surface water samples. The O_2 distribution is based on World Ocean Atlas 2013 data. The plot was produced with Ocean Data View software (R. Schlitzer, 2018).

Cadmium isotope ratios were measured by thermal ionization mass spectrometry using a Triton (ThermoFisher) instrument. Raw data were corrected for instrumental mass bias using a double-spike reduction algorithm and assuming an exponential fractionation law (see A.-D. Schmitt et al., 2009). Cadmium concentrations were determined by isotope dilution using the method described in Xie et al. (2015) with a reproducibility better than 1%. For the FISH samples, the chemical separation of Cd follows the method described by Xie et al. (2017). The $^{112}Cd/^{110}Cd$ isotopic ratios were measured and are expressed as $\varepsilon^{112/110}Cd$ relative to NIST SRM-3108:

$$\varepsilon^{\frac{112}{110}}Cd = \left(\frac{\left(\frac{^{110}Cd}{^{112}Cd}\right)_{\text{NIST SRM 3108}}}{\left(\frac{^{110}Cd}{^{112}Cd}\right)_{\text{sample}}} - 1 \right) \times 10,000 \quad (1)$$

The data are listed in Tables S1–S3 and in the figures in the de facto current conventional $\delta^{114}Cd$ notation (in parts per thousand, ‰) using the conversion factor of 0.2000425 reported by Abouchami et al. (2013). Repeated analyses of the NIST SRM-3108 international standard yielded a $^{110}Cd/^{112}Cd$ ratio of 0.520120 ± 0.000014 (2σ, $n = 66$, $\delta^{114}Cd = 0.00 \pm 0.05$‰), in agreement with previous studies carried out in the same laboratory (W. Abouchami et al., 2011; D. J. Janssen et al., 2017; R. C. Xie et al., 2017). The long-term external reproducibility of Cd isotope composition, based on five replicates of seawater samples previously published (W. Abouchami et al., 2011; W. Abouchami et al., 2014), is ±0.04‰ (see Table S2). The procedural blanks performed on 1, 4 and 10 L volumes of de-ionized water (Milli-Q, Merck Millipore) were 4.2, 5.8 and 2.3 pg Cd, respectively, and have a negligible impact on Cd isotopic compositions (Table S2).

3. Results

3.1. Distribution of Cadmium Concentrations and $\delta^{114}Cd$ in the Angola Basin

Cadmium concentrations and isotope compositions measured on seven vertical profiles and corresponding surface water samples are plotted in Figure 3 and show distribution patterns similar to those observed elsewhere in the Atlantic Ocean (W. Abouchami et al., 2014; Conway & John, 2015b; R. C. Xie et al., 2018; R. C. Xie et al., 2017). Depth profiles of Cd and PO_4 concentrations exhibit strong similarities (Figure S4). Interestingly, the Cd/PO_4 ratio varies slightly between water masses (Figure 4) with lower values (0.225–0.243 nmol/µmol) for NADW than those of Southern Ocean-derived water masses (0.244–0.315

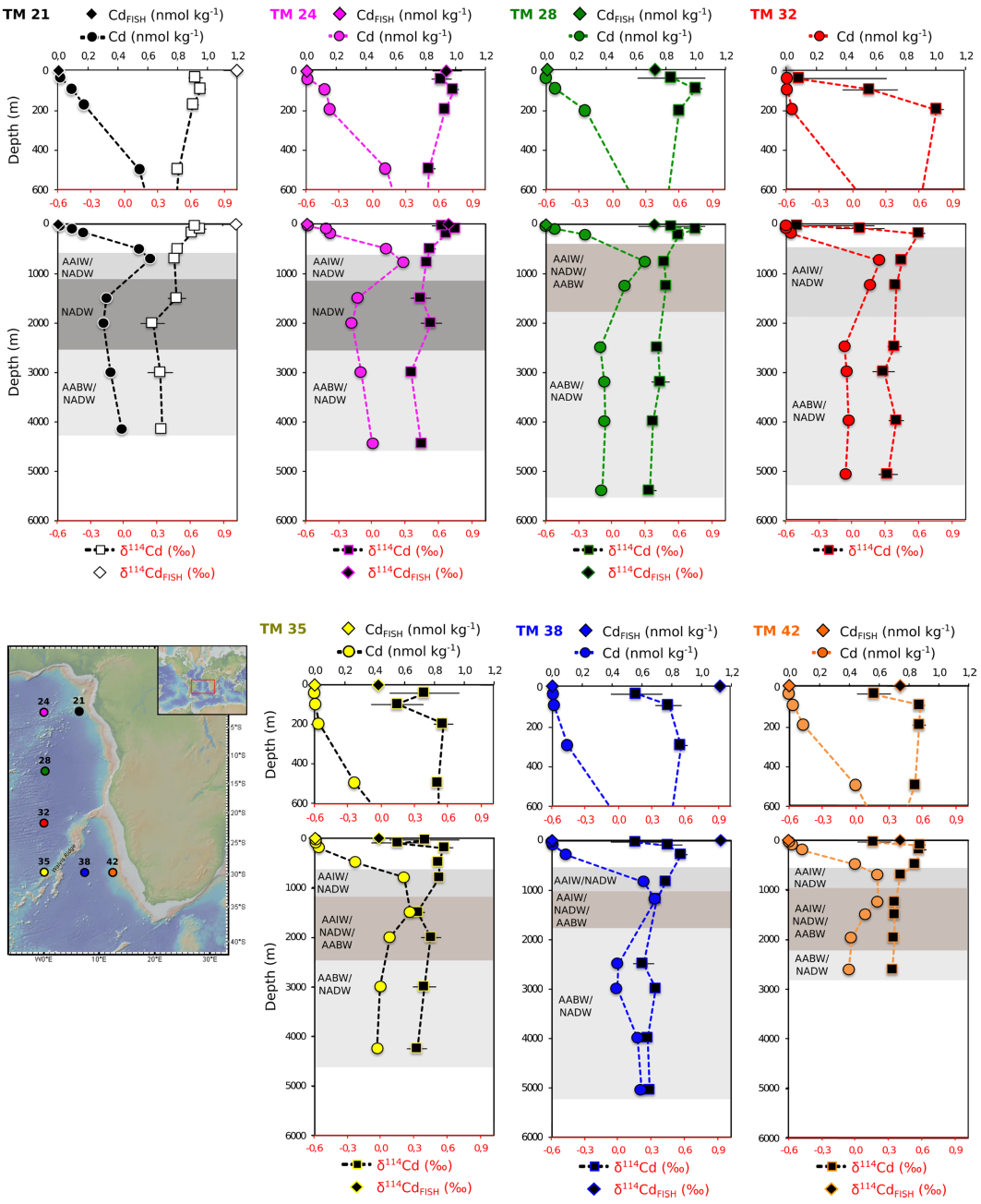

Figure 3. Depth profiles of Cd concentrations and isotope compositions in the Angola Basin. The FISH samples (diamonds) were not strictly obtained at the same locations as the vertical profiles, but each FISH sample data point was associated in this figure to the nearest vertical profile. The color codings of the station locations are shown on the map (left bottom). Error bars for Cd concentrations and δ^{114}Cd are smaller than symbol size, unless visible.

nmol/μmol for AABW and 0.268–0.308 nmol/μmol for AAIW), in agreement with previous observations in the Atlantic (W. Abouchami et al., 2014; O. Baars et al., 2014; R. Middag et al., 2018; P. Quay et al., 2015). The data display an exponential Cd depletion (down to 0.2 pmol/L at TM 32) in the upper 200 m of surface waters, which is stronger in the southern part of the basin (TM 32 to TM 42). The heaviest δ^{114}Cd signatures are measured at around 100–200 m depth in each profile. Lighter and more variable Cd isotope signatures are found at stations (TM 35, 38, and 42) located south of station TM 32, compared with those (TM 21, 24, and 28) inside the perimeter of the Angola ODZ.

As expected, the surface FISH samples are strongly Cd depleted (0.001–0.006 pmol/L) with δ^{114}Cd ranging from −0.04‰ to 1.02‰, in line with published data (R. C. Xie et al., 2017, 2018) from the western part of the

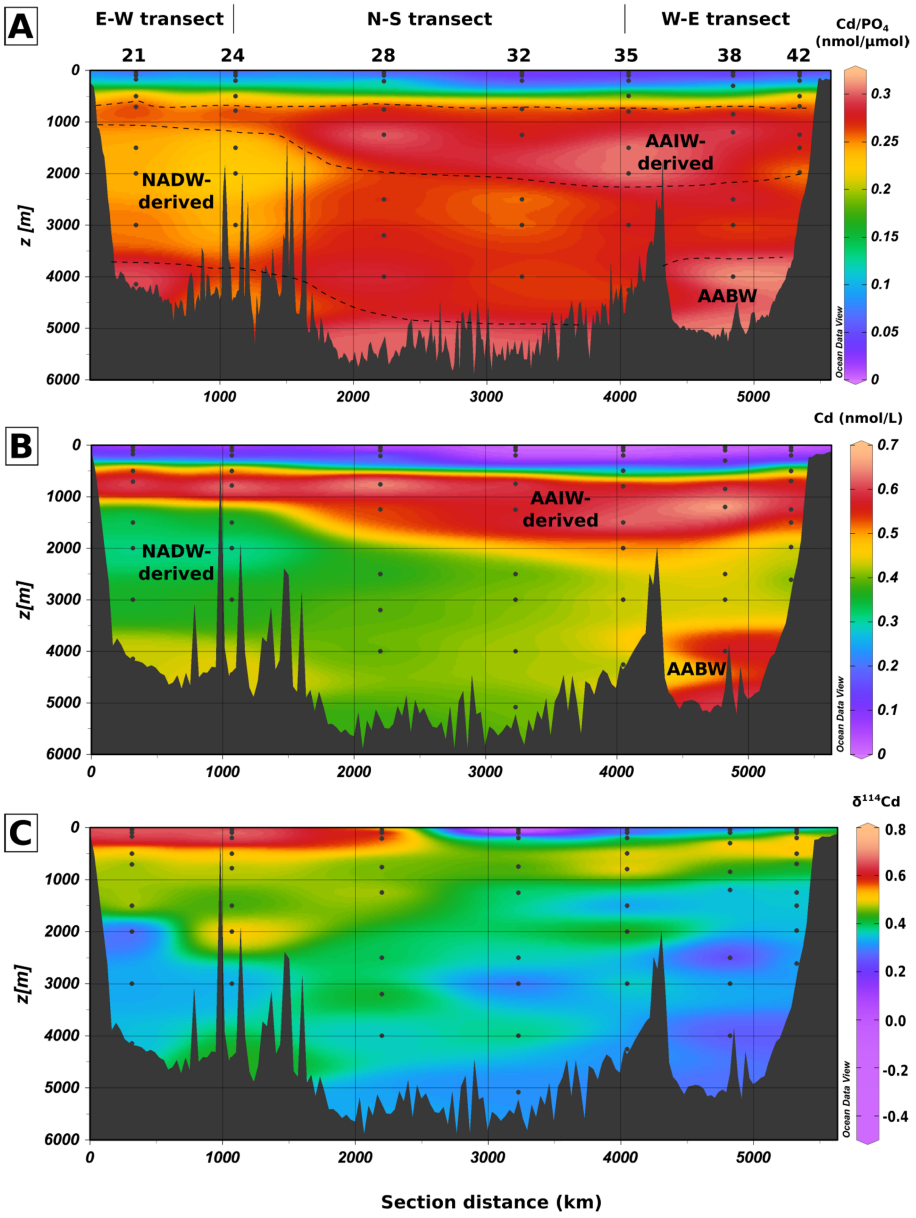

Figure 4. Cross section of interpolated Cd/PO_4 ratio (4a), Cd concentrations (4b), and $\delta^{114}Cd$ (4c) along the section shown in Figure 1. The acronyms AAIW, NADW, and AABW refer to Antarctic Intermediate Water, North Atlantic Deep Water, and Antarctic Bottom Water, respectively. The plot has been realized with the Ocean Data View software (R. Schlitzer, 2018).

South Atlantic (see Figure 6b). Extremely heavy Cd isotopic compositions with $\delta^{114}Cd$ up to 5‰ as reported in the North Atlantic transect (Conway & John, 2015b), are not observed in our data set.

The tongue of low salinity and Cd-enriched AAIW is located between 500 and 1,300 m depth in the northern part of the transect and deepens to 800 to 2,100 m depth in the southern part of the basin (Figure 4) The $\delta^{114}Cd$ ranges from 0.32‰ and 0.51‰, in agreement with the isotope signature of AAIW ($\delta^{114}Cd$ of 0.45 ± 0.08‰) based on literature data compiled by Xie et al. (2017). Below, NADW is characterized by a maximum extent of 2,500 m at stations TM 28 and TM 32 and lower Cd concentrations than those of AAIW, whereby the values increase southward from 0.31 to 0.45 nmol/L, reflecting progressive mixing and dilution with AABW within the RFZ. The associated $\delta^{114}Cd$ ranges from 0.22‰ to 0.51‰ with heavier values found in the north (TM 21 and TM 24). The slight increase in Cd concentrations at the bottom of TM 21 and TM 24 (Figure 4) can be attributed to a stronger proportion of AABW relative to NADW in this northern part

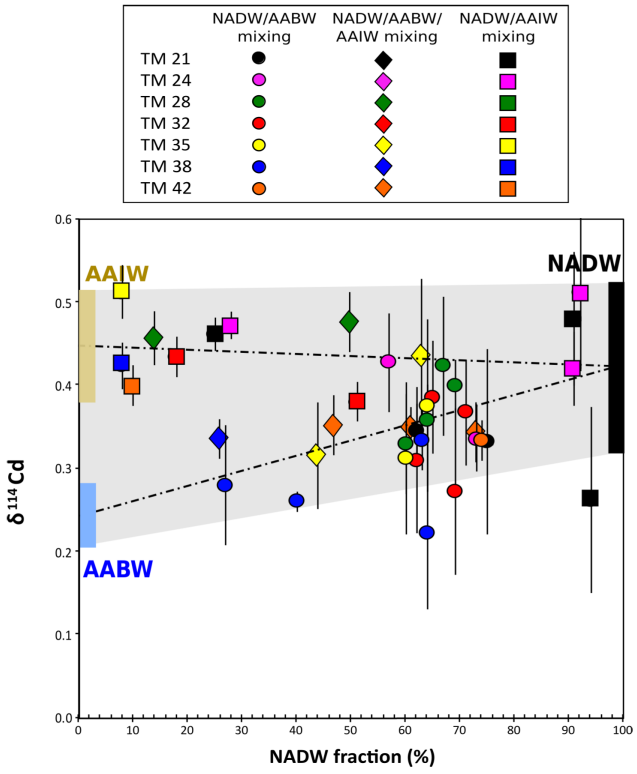

Figure 5. Conservative mixing of δ^{114}Cd in the deep Angola Basin (>750 m depth). The proportion of NADW in the mixing is calculated using the e-OMP model, whereas the end-member δ^{114}Cd was obtained from the literature (W. Abouchami et al., 2014; R. C. Xie et al., 2017; Z. Xue et al., 2013). The samples controlled by binary mixing between NADW and AABW or between NADW and AAIW are displayed by dots and squares, respectively. Diamonds represent samples impacted by contributions from all three water masses.

of the basin (Figure S2, Stramma & England, 1999). The higher Cd concentration and lower δ^{114}Cd measured at depth at the station TM 38 profile reflects the presence of "pure", unaltered AABW corresponding to the southern branch of AABW flow into the south Atlantic (see Figure S2).

4. Discussion

4.1. Cadmium Cycling in Deep Waters: Dominant Control by Water Mass Mixing

The deepwater distributions of Cd concentrations and isotopic compositions are mainly controlled by mixing between water masses with preformed signals (W. Abouchami et al., 2014; R. C. Xie et al., 2017). The bilinear relationship between Cd and PO_4 has recently been interpreted as reflecting dominantly water mass mixing whereby only 10–30% of the total Cd can be accounted for by particle regeneration following sinking (R. Middag et al., 2018). Likewise, the Cd isotope distribution in Angola Basin deepwater shown in Figure 4 appears to be largely governed by water mass mixing with superimposed influence from regeneration of sinking organic particles.

Following the methodology of Middag et al. (2018), we use an extended Optimum Multiparameter Model (e-OMP) (Karstensen & Tomczak, 1998) to, first, infer the relative importance of water mass mixing and remineralization processes in the Angola Basin on Cd concentrations and δ^{114}Cd, and second, determine the respective proportions of the three main water mass components—AABW, NADW, and AAIW. These are defined, according to literature and property-property plots, by their temperature, salinity, and oxygen content as well as silicate, phosphate, and nitrate concentrations (see Table S3). The remineralization of organic particles is also considered in this model and will mostly occur in the depth range of AAIW (500–1,300 m depth). The extent of the remineralization process is expressed as an oxygen deficit (DO_2) as in Middag et al. (2018). Practically, the DO_2 deficit value is the difference between the O_2 concentration determined solely by conservative mixing between two or three water masses and the observed O_2 concentrations. Remineralization ratios $\Delta P{:}\Delta N{:}\Delta O_2$ of 1:16:170 were chosen following Anderson and Sarmiento (1994), whereas $\Delta Si{:}\Delta O_2$, even if variable vertically, was fixed at 1:34 following Middag et al. (2018). The relative weight of each input parameter was calibrated to obtain a minimum data residue after the fit. After model processing, calculated Cd concentrations were determined as

$$Cd_{calc} = f_{AABW}Cd_{AABW} + f_{NADW}Cd_{NADW} + f_{AAIW}Cd_{AAIW} + DO_2 \times (Cd : O_2)_{remin} \quad (2)$$

with f and Cd corresponding to the proportion and Cd concentrations of AABW, AAIW, and NADW in the mixing, respectively. The endmember Cd concentrations used are those reported by Xie et al. (2017) and Middag et al. (2018) (Table S3). The $(Cd{:}O_2)$ remineralization ratio of 1.5:1, obtained after optimization of the calculated versus observed Cd fit (Figure S5a), range between the values reported by Middag et al. (2018) ($Cd{:}O_2$ of 1.25:1) and those of Roshan and Wu (2015) ($Cd{:}O_2$ of 2:1). The δ^{114}Cd of regenerated Cd is still poorly constrained in the literature and is expected to be close to that of AAIW (D. J. Janssen et al., 2019; M. Sieber et al., 2018). The calculated δ^{114}Cd is thus only based on conservative mixing between the water masses in question, namely,

$$Cd_{calc}\delta^{114}Cd_{calc} = f_{AABW}Cd_{AABW}\delta^{114}Cd_{AABW} + f_{NADW}Cd_{NADW}\delta^{114}Cd_{NADW} + f_{AAIW}Cd_{AAIW}\delta^{114}Cd_{AAIW} \quad (3)$$

The Cd concentrations and δ^{114}Cd of the NADW, AABW, and AAIW water mass endmembers were obtained from the literature (W. Abouchami et al., 2014; O. Baars et al., 2014; R. Middag et al., 2018; R. C. Xie et al., 2017) and are reported in Table S3. The AABW is Cd-rich (Cd = 0.78 nmol/kg) with light

δ^{114}Cd (0.25 ± 0.04‰) as it is formed by subduction of Circumpolar Deep Water (CDW), for which Cd consumption is incomplete (W. Abouchami et al., 2014; Z. Xue et al., 2013). A small portion of this Cd-rich upwelled Circumpolar Deep Water is also delivered to the surface and flows northward contributing to AAIW, which is characterized by comparatively moderate Cd concentration (Cd = 0.53 nmol/kg) and heavier δ^{114}Cd (0.45 ± 0.08‰) due to higher biological Cd consumption. Finally, the δ^{114}Cd signature of Cd-poor NADW (Cd = 0.215 nmol/kg) is heavy (0.42 ± 0.10‰) and mainly controlled by the mixture of waters of North Atlantic and Arctic origin and Southern Ocean origin (namely, AAIW) (M. Lambelet et al., 2013; S. Ripperger et al., 2007; R. C. Xie et al., 2017).

The model was applied only for depths below 750 m based upon three lines of argumentation. First, the Angola Basin ODZ lies between 200 and 600 m depth. As CdS precipitation is expected in this zone, the measured Cd concentrations and δ^{114}Cd in the ODZ will be the result of conservative mixing of a regenerated Cd and of a CdS-sequestered component. Second, the physical and chemical characteristics of subsurface waters in the Angola Basin are poorly constrained since they are strongly affected by biological cycling. Third, the remineralized Cd/PO_4 ratio was recently shown to vary in the top 700 m of an ETSP transect (*S* Roshan et al., 2017), making it difficult to quantify the proportion of regenerated Cd in the upper 700 m of the water column.

The proportion of each water mass involved in the mixing and the importance of remineralization along the section defined in Figure 1 are illustrated in Figure S6. The proportion of remineralized Cd accounts for approximately 30% and 10% of the total Cd below 700 and 2,000 m depth, respectively (Figure S5b), supporting a predominant water mass mixing control on the deepwater Cd isotope signature. The measured δ^{114}Cd for samples below 700 m depth is fully consistent with mixing (Figures 5 and S7) between AABW and NADW (dots); AAIW and NADW (squares); and NADW, AAIW, and AABW (diamonds). Interestingly, the addition of remineralized Cd in the 700 to 1,300 m depth range does not seem to induce drastic changes in the δ^{114}Cd signature of AAIW. Based on the measured values of δ^{114}Cd (0.6–0.8‰) in surface waters (Figure 6a), and assuming a Cd isotope fractionation factor $\alpha^{114/110}$Cd of 1.0005 between seawater and particles (R. C. Xie et al., 2017), the isotope signature of the particulate Cd released by remineralization can be constrained to 0.36‰ to 0.56‰. Since remineralized Cd does not represent more than 30% of the total Cd—thus inducing a maximum shift of 0.06–0.08‰—its effects will not be significant for the deepwater Cd isotope signature. A similar conclusion was reached in the Southwest Pacific, where the delivered remineralized Cd was found to have a Cd isotope signature close to that measured in AAIW thereby accounting for the stability of equatorial AAIW δ^{114}Cd along the transect (M. Sieber et al., 2018).

The relative stability of Cd cycling in subsurface waters is also reflected by the distribution of Cd concentrations. Indeed, the best fit for the e-OMP model is obtained with a remineralization Cd/PO_4 ratio of 0.255, which is in the range of measured Cd/PO_4 ratio in AAIW (Cd/PO_4 = 0.22–0.32, O Baars et al., 2014; P. A. Yeats et al., 1995; this study) that can be considered as the main source of Cd and PO_4 to the surface waters. This constant remineralized Cd/PO_4 ratio is also in line with that reported by Roshan and Wu (2015) (Cd/PO_4 = 0.262) to model the Cd-PO_4 relationship below 300 m depth in the North Atlantic or with the relatively stable regenerated Cd/PO_4 calculated for depth below 700 m in the ETSP ODZ, where regenerated Cd is the main source of dissolved Cd (S. Roshan et al., 2017). This finding contrasts, however, with the variability of Cd/PO_4 ratio and associated δ^{114}Cd of regenerated organic material observed in particles in the upper water column, which has been explained by differential remineralization efficiencies of "soft" and "protected" sinking particles (O. Baars et al., 2014; D. J. Janssen et al., 2019; Wu & Roshan, 2015).

In summary, even if a strong surface Cd and PO_4 depletion occurs in the Angola Basin (Figure 3), the similarity of Cd/PO_4 ratios of AAIW-sourced water and remineralized materials below 700 m depth at all stations is consistent with uniform subsurface cycling, as has been assumed in the South Atlantic (R. Middag et al., 2018) and South Pacific (M. Sieber et al., 2018). Nevertheless, studies focusing on the biogeochemical cycling of Cd in the surface layer are needed to evaluate the validity of this hypothesis.

4.2. Cd Cycling in the Surface Waters: What is the Controlling Factor?

The surface water samples from the Angola Basin do not exhibit δ^{114}Cd higher than 1.02‰, which is similar to results of recent Cd isotope studies in the South Atlantic and tropical Atlantic Ocean (R. C. Xie et al., 2017, 2018) as well as the Pacific Ocean (D. J. Janssen et al., 2017; M. Sieber et al., 2018; R. C. Xie et al., 2019). This

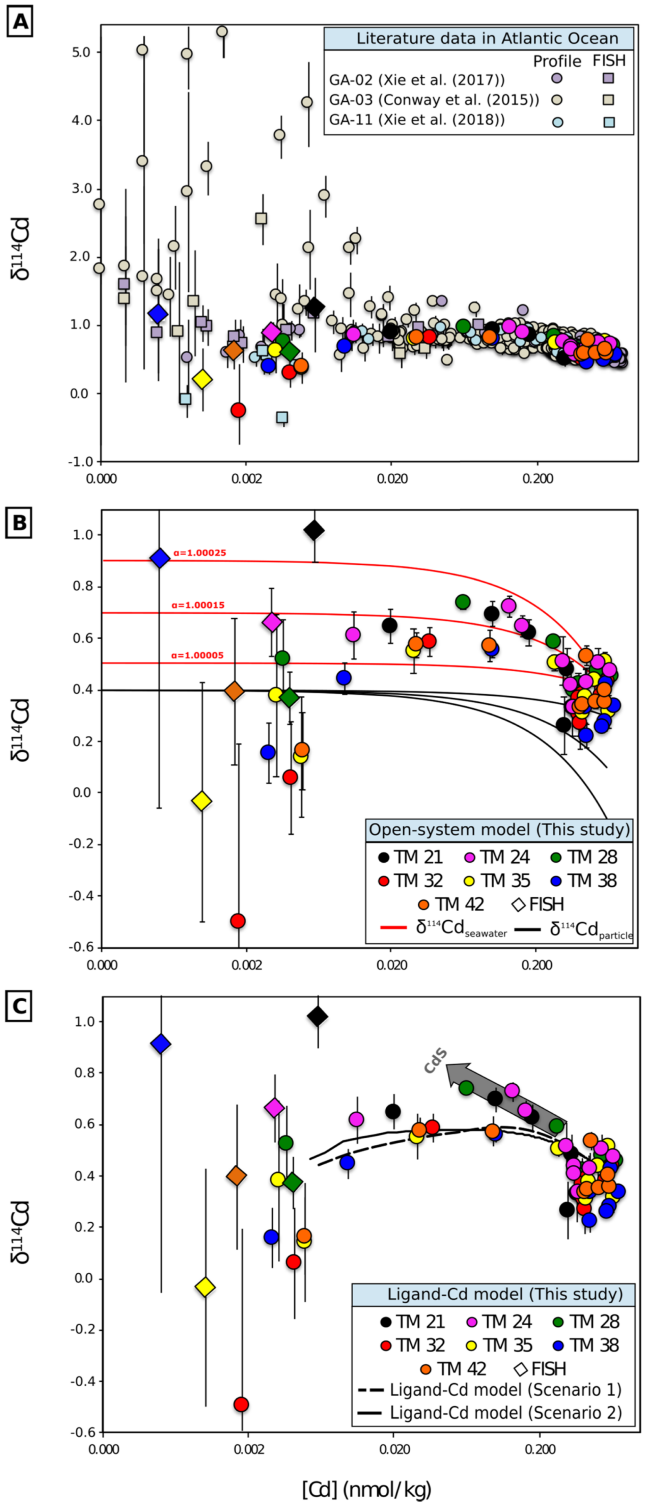

Figure 6. Cadmium isotope systematics in the Atlantic Ocean. (a) Compilation of published Atlantic Ocean Cd isotope data (Conway & John, 2015b; R. C. Xie et al., 2017, 2018; this study). The data from vertical profiles (dots) and surface (FISH, squares for the literature data and diamonds for this study) samples analyzed in this study are included in the three figures. The color of FISH sample symbol is associated with the color of the closest vertical profile. (b) The red and black lines refer to the evolution of modeled Cd concentrations and isotope signatures in seawater and particles, respectively. The $\alpha^{114/110}$ values refer to the fractionation operating between seawater and particles. (c) The black straight and dashed lines depict the Cd-ligand model output for the two tested scenarios. In b and c, the initial conditions are a Cd concentration and a δ^{114}Cd in seawater of 0.6 nmol/L and 0.40‰, respectively, in agreement with the values observed at 900 m depth, the location of the maximum remineralization zone within AAIW.

contrasts with the heavy δ^{114}Cd (up to 5‰) observed in the upper 100 m layer in the North Atlantic (Conway & John, 2015b) and North Pacific (S. Ripperger et al., 2007) (Figure 6a). The lack of highly fractionated Cd isotope signatures and relatively homogeneous surface δ^{114}Cd has been attributed to either diffusion under supply-limited conditions with respect to phytoplankton uptake (M. Gault-Ringold et al., 2012; E. George et al., 2019), or to an open steady-state system or Cd complexation by organic ligands (R. C. Xie et al., 2017). The supply-limited model can possibly explain the quasi-constant δ^{114}Cd found in surface waters of the Angola Basin. In the surface ocean, inorganic Cd concentrations will be lower than 1 pmol/L, the defined threshold of a supply-limited regime (F. M. M. Morel, 2008), as ligand complexed Cd is the dominant species of dissolved Cd.

Our data can also be described in terms of a steady-state model with an $\alpha^{114/110}_{\text{solution}-\text{particle}}$ varying from 1.0001 to 1.0005 (Figure 6b). However, both models cannot account straightforwardly for the low δ^{114}Cd of Cd-depleted samples at stations TM32 to TM42. The evolution of Cd concentrations and isotopes in the subsurface Angola Basin can, however, be reproduced using a combination of an open steady-state system and a Cd-ligand complexation model as detailed in the supporting information (Text S1). Briefly, the decrease in total Cd (Cd_T) concentrations from 900 m to the surface is assumed to affect mostly the available inorganic Cd pool (hereafter Cd′) within an open steady-state system as described by Xie et al. (2017). In our model, Cd is removed with decreasing depth in a hundred incremental steps over the whole depth profile; 1% of Cd_T (6 pmol/L) is removed in 1% of the total depth, that is, 9 m. After each incremental removal of Cd′, we calculate the proportion of Cd_L that must be transferred to the Cd′ pool to satisfy the thermodynamic equilibrium between Cd′ and the ligand-bound Cd (Cd_L hereafter) species in solution. Cadmium complexation or desorption from organic ligands is not expected to induce an isotope fractionation as deduced from data obtained during degradation experiments of *D. tertiolecta* (John & Conway, 2014). Thus, at the initial stage at 900 m depth, Cd′ and Cd_L have a similar δ^{114}Cd of 0.40‰, which corresponds to the average value observed in the range 700–900 m depth in our vertical profiles.

The removal of Cd′ in an open system at steady state is associated with an isotope fractionation factor of $\alpha^{114/110}$Cd of 1.0005 between solution and particles, as in Xie et al. (2017), enriching the remaining dissolved Cd in heavy isotopes. This fractionation factor is of a similar magnitude to that observed in the 100–700 m depth range in the northeast and northwest Pacific between particles and seawater where an offset of 0.6‰ to 1.0‰ between light Cd in particles and heavy Cd in solution was measured (D. J. Janssen et al., 2019; S.-C. Yang et al., 2018). Janssen et al. (2019) showed that the Cd isotope fractionation associated with Cd uptake by phytoplankton in the photic zone is limited and the shallow remineralization of 90% of organic particles with heavy Cd isotope composition results in a downward export of more refractory particles with lighter δ^{114}Cd. The final transfer of dissolved Cd from Cd_L to the Cd′ pool to balance the thermodynamic equilibrium in solution induces a buffering of the heavy dissolved $\delta^{114}Cd_T$ as $\delta^{114}Cd_L$ of the Cd-ligand pool remains stable at 0.40‰.

Two different scenarios were tested by varying the concentration and complexation constant of the Cd-specific organic ligands on the basis of previous studies (Bruland, 1992; Baars, unpublished data). The results of the open-system ligand-bound Cd combined model for both scenarios are illustrated in Figure 6c and agree reasonably well with the evolution of Cd systematics in our study region, especially at low Cd concentrations. The simulation does not apply for Cd concentrations lower than 4 pmol/L which are typically found in the top 10–20 m surface waters where other processes, such as biological uptake, sorption on organic particles, a supply-limited regime, or shallow remineralization, may act separately or together to complicate the behavior of the system.

In summary, the Cd isotope systematics in the subsurface ocean can be explained best by combining the open-system model and the buffering role played by Cd-ligand complexation. Additionally, this simulation shows that the samples located inside the ODZ are offset from the main trend in Figure 6c, with more elevated δ^{114}Cd signatures than expected, hinting at the involvement of additional processes. We will argue below that this is most likely CdS precipitation.

4.3. Occurrence of Cadmium Sulfide Precipitates in the Angola Basin ODZ

The potential role of cadmium sulfide precipitates in Cd isotope fractionation in ODZs was first proposed by Janssen et al. (2014) based on (1) the observation of a Cd depletion relative to PO_4 combined with (2) an

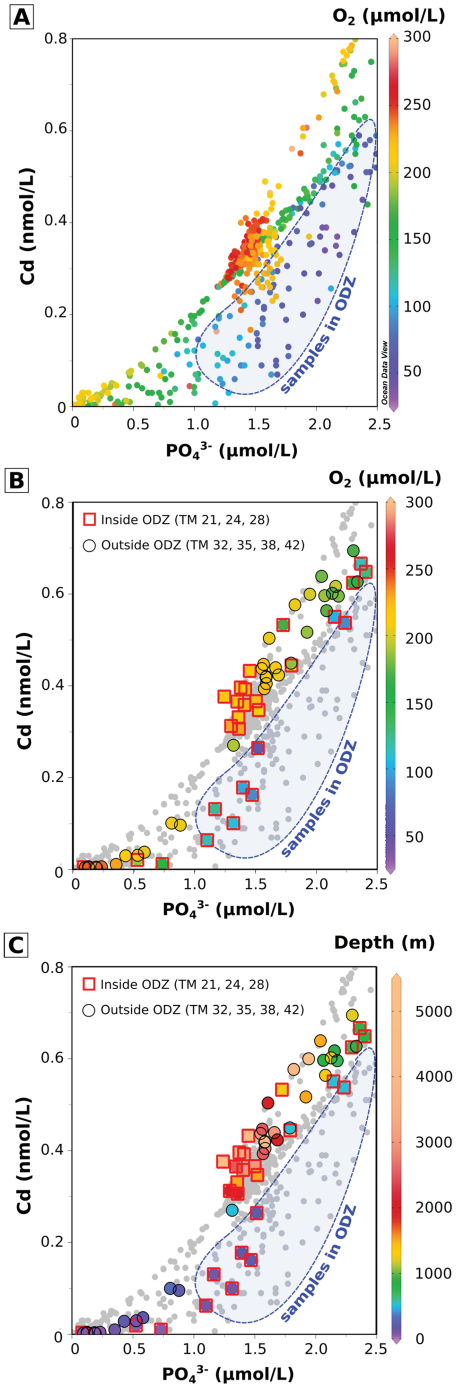

Figure 7. Cadmium-phosphate relationship in the Atlantic Ocean. (a) Compilation of Cd and PO_4 concentrations from the North Atlantic GA-03 and GA-11 transects within the Mauritanian ODZ area (Conway & John, 2015b; R. C. Xie et al., 2018), from the Congo-Angola Biozaire 3 transect where the Angola Basin ODZ is located (M. Waeles et al., 2013) and from the GA-02 transect, not affected by any ODZ (R. C. Xie et al., 2017). (b and c) Cd and PO_4 concentrations from this study. The samples from the seven profiles are distinguished as inside ODZ profiles (TM21, TM24, and TM28) or outside ODZ profiles (TM32, TM35, TM38, and TM42). The *z* axis represents the O_2 concentrations (b) and the sampling depth (c) of the samples. The plot was realized with Ocean Data View software (R. Schlitzer, 2018).

enrichment in heavy Cd isotopes in the dissolved pool, alongside (3) an enrichment in particulate Cd relative to PO_4. The occurrence of particulate Ba in the Mauritanian ODZ due to barite precipitation supports the CdS hypothesis given that these two species are known to precipitate in similar microenvironments (S. L. Bates et al., 2017; Conway & John, 2015b; T. J. Horner et al., 2015).

The available Cd-PO_4 data set for the Atlantic Ocean is plotted in Figure 7a and clearly shows a Cd depletion compared to PO_4 in O_2 deficient waters within the Mauritanian (Conway & John, 2015b) and Angola Basin ODZs (M. Waeles et al., 2013). To assess the degree of Cd depletion, if any, in our samples, the seawater profiles are subdivided according to their location within the ODZ ("inside" shown as red squares, TM21, TM24, and TM28) and outside the ODZ ("outside" shown as black dots, TM32, TM35, TM38, and TM42). It can be seen in Figure 7b that most of our samples plot close to the regression line defined by fully oxygenated Atlantic waters. However, all six low-oxygen samples from within the ODZ between 200 and 600 m depth (Figure 7c) exhibit significant Cd depletions relative to PO_4 and plot within the ODZ field area defined in Figure 7b.

The Cd* parameter (O. Baars et al., 2014; D. J. Janssen et al., 2014) has been used as a tracer of relative Cd depletion or excess and is defined as

$$Cd^{*} = Cd_{measured} - (Cd/PO_4)_{deep} \times PO_{4measured} \quad (4)$$

However, the Cd* notation, and especially the assumption of a given constant $(Cd/PO_4)_{deep}$, can be misleading due to the variability of Cd/PO_4 ratios within the same water mass, in particular, in ODZs where CdS precipitation may occur (R. Middag et al., 2018; R. C. Xie et al., 2019). This limits the utility of this tracer alone and requires inclusion of another independent parameter, as discussed by Xie et al. (2019). Following Conway and John (2015b), we combine Cd* values and δ^{114}Cd signatures—a quasi-conservative feature of water masses—which, unlike Cd and PO_4 concentrations, is unaffected by variable regeneration.

The identification of the occurrence of CdS precipitates is only unambiguous if there is a significant shift of δ^{114}Cd toward heavier values associated with a pronounced negative Cd*, reflecting a strong Cd depletion largely exceeding that expected from the variability in the chosen $(Cd/PO_4)_{deep}$ ratios. To evaluate the effects of the latter on calculated Cd* values, four different scenarios were considered whereby $(Cd/PO_4)_{deep}$ was inferred from (1) only samples below 700 m depth ($n = 36$); (2) samples below 1,250 m depth ($n = 25$); (3) only samples resulting from NADW-AABW mixing ($n = 23$), and (4) only mixtures of AAIW and NADW ($n = 14$). For Cases 1 to 4, $(Cd/PO_4)_{deep}$ varies between 0.264 ± 0.028 and 0.284 ± 0.019 and results in a total Cd* variation of only ±0.03. This variation is by far smaller than the uncertainty (10–11%) of the intrasample variability in the Cd/PO_4 ratio. This clearly demonstrates that the distinct Cd/PO_4 ratios of individual water masses cannot be solely responsible for generating the trend in δ^{114}Cd vs Cd* seen in Figure 8. Furthermore, the area studied is sufficiently far from the coast to not be influenced by inputs of PO_4 from the continental margin, as argued for the Amazon River plume in the Southwest Atlantic (R. C. Xie et al., 2018). The relationship between δ^{114}Cd and Cd* shown in Figure 8 thus

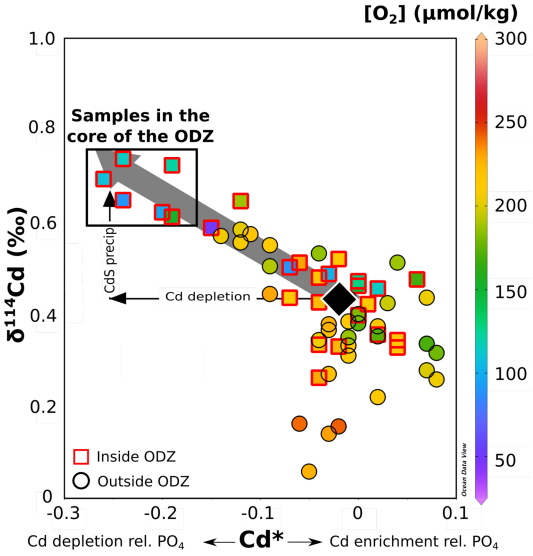

Figure 8. Shift of cadmium isotope compositions as a consequence of CdS precipitation. The calculation of the theoretical Cd isotope shift associated with the Cd depletion induced by CdS precipitation is reported as a gray arrow. The black rectangle represents the samples from within the core of the ODZ. The samples from the seven profiles are subdivided into those inside the ODZ area (TM21, TM24, and TM28) and outside the ODZ area (TM32, TM35, TM38, and TM42). The *z* axis represents the O_2 concentrations of the samples. The plot was realized with this Ocean Data View software (R. Schlitzer, 2018).

most likely reflects the presence of CdS precipitates in the oxygen deficient waters of the Angola Basin.

As seen in Figure 8, samples located in the core of the ODZ show maximum Cd depletion and are associated with the heaviest δ^{114}Cd values—features that are not observed for the samples outside the ODZ. In order to assess whether there is a causal relationship between δ^{114}Cd enrichment and the presence of CdS precipitates, we calculate a theoretical δ^{114}Cd value for a maximum Cd depletion in the water. This uses the Cd isotope fractionation factor recently determined experimentally for CdS precipitation in synthetic seawater ($\alpha^{114/110}Cd_{sol}$-CdS = 1.00032, D. Guinoiseau et al., 2018). The δ^{114}Cd of the Cd-depleted water is obtained from:

$$\delta^{114}Cd = \left(\delta^{114}Cd_{ini} + 1,000\right) \times \left(f^{\left(1-\alpha 114/110_{Cdsol-CdS}\right)}\right) - 1,000 \quad (5)$$

where $\delta^{114}Cd_{ini}$ is the initial value and f corresponds to the proportion of dissolved remaining Cd.

Since CdS precipitation is expected to occur in the ODZ at depths occupied by AAIW, we adopted the mean Cd isotopic composition of AAIW (δ^{114}Cd = 0.45 ± 0.08‰; Xie et al., 2017) for $\delta^{114}Cd_{ini}$, which is slightly heavier than that of local deepwater (δ^{114}Cd = 0.37 ± 0.08‰).

The calculated values are in good agreement with the Cd isotope signatures measured within the ODZ (end of the gray arrow in Figure 8) indicating that CdS precipitation within sinking particles very likely occurs within the Angola Basin ODZ. Similar calculations performed on data obtained for the Mauritanian (Conway & John, 2015b) and the ETSP ODZ (S. G. John et al., 2017) agree well with the reported δ^{114}Cd-Cd* relationship in these studies, suggesting that CdS is formed there as well (details can be found in D. Guinoiseau et al., 2018). We conclude that CdS precipitation may play a significant role in the biogeochemical cycling of Cd in ODZs worldwide and is thus of global rather than local importance. However, in the North Pacific ODZ, where conditions seem *a priori* favorable for CdS precipitation, there is no Cd isotopic evidence of such a process—namely no shift in δ^{114}Cd has been observed in association with more negative Cd* (D. J. Janssen et al., 2017). The analysis of particulate δ^{114}Cd in the North Pacific ODZ indicates that the main process affecting Cd isotope systematics in this region is the mineralization of organic particulate matter, blurring any Cd*-δ^{114}Cd effects due to CdS precipitation (D. J. Janssen et al., 2019). Clearly, there are many factors influencing CdS precipitation within sinking particles and it should be a priority of future studies to better constrain the impact of this process on the global oceanic Cd cycling.

4.4. Implications of CdS Precipitation Processes in the Global Oceanic Cd Cycle

As discussed above, CdS precipitation is likely to occur in three distinct ODZs, namely, that off Mauritania, the ETSP, and the Angola Basin. In these systems, the formation of CdS reaches its maximum between 100 and 200 m water depth in the uppermost parts of the low-oxygen layers (Figure 9a) and not necessarily at the depth of the O_2 minimum, which is located at 300–500 m water depth in the Mauritanian and Angola Basin ODZ (Figure 9b). Therefore, the O_2 depletion of seawater below a defined threshold is not the sole factor controlling the precipitation of CdS within the microenvironment of sinking biogenic particles but must also be influenced by locally favorable water column conditions.

A particle size-resolved model developed by Bianchi et al. (2018) indeed shows that bacterial sulfate reduction likely occurs at the transition between the oxycline and the ODZ (100–300 m depth) within >1 mm diameter particle aggregates that release H_2S leading to the formation of the CdS precipitates. The depth profiles of particulate Cd and Cd/PO_4 generated by this model are in perfect agreement with observations from the Mauritanian ODZ (Conway & John, 2015b; D. J. Janssen et al., 2014). The model also suggests that the main oceanic ODZs—located in the Arabian Sea, South Pacific, the Angola Basin and ETSP—are locations of

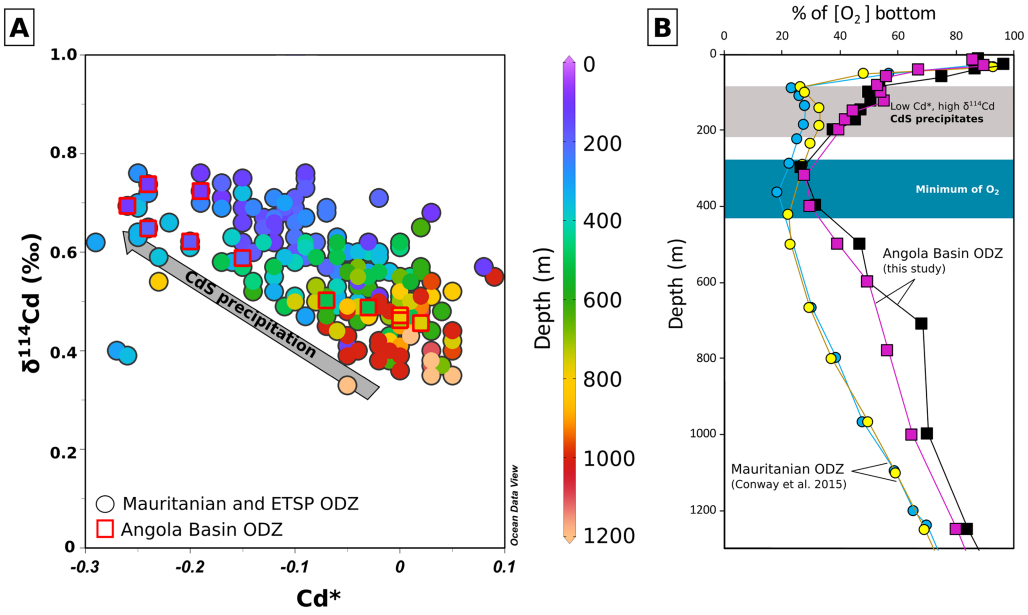

Figure 9. Depth of CdS precipitation within oceanic ODZs. (a) Evolution of δ^{114}Cd and Cd* in the three oceanic ODZ sections where CdS precipitation has been proposed to occur (Conway & John, 2015b; D. J. Janssen et al., 2014; S. G. John et al., 2017). Only data with O_2 concentration below 150 μmol/L and a water depth below 100 m were reported here to remove potential effects of biological uptake in surface waters. The z axis reflects the depth of the samples. (b) Vertical oxygen distribution in USGS 10 TM9 and TM10 profiles located in the core of the Mauritanian ODZ (Conway & John, 2015b) and in TM21 and TM24 profiles located in the Angola Basin ODZ. The maximum of CdS precipitation is assumed to occur when Cd* is the lowest and δ^{114}Cd the highest (gray area). A decoupling between the CdS precipitation area and the O_2 concentration minimum (blue area) is clearly visible. The plot was realized with the Ocean Data View software (R. Schlitzer, 2018).

intensive sulfate reduction, in agreement with the systematic evident in the distribution of Cd concentrations and its isotopes compiled and discussed by Guinoiseau et al. (2018). In contrast, the lack of evidence for CdS precipitation in the North Pacific ODZ—such as a strong Cd depletion or a shift of δ^{114}Cd (D. J. Janssen et al., 2017)—might be explained by the absence of sulfate reduction which, according to the model of Bianchi et al. (2018), is a necessary precursor for CdS precipitation.

The key role played by sulfate reduction in CdS formation is also supported by biological evidence of an active sulfur cycle within the ODZ. A cryptic sulfur cycle has been proposed within the ETSP ODZ based on the identification of sulfide oxidizing and sulfate reducing bacterial strains that can account for one third of the organic carbon remineralization in ODZ environments (D. E. Canfield et al., 2010). Genomic sequencing shows maximum diversity near the upper boundary of the South Pacific ODZ where active S-cycling groups like *Chromatiales* are observed (Beman & Carolan, 2013; M. T. Carolan et al., 2015). Likewise, sulfate-reducing (*Desulfosarcina* or *Desulfofrigus*) and sulfide-oxidizing (*Riftia* or *Calyptogena*) bacteria have been isolated in the Arabian Sea ODZ (B. M. Fuchs et al., 2005). Observations of trace metal enrichments, including Cd, relative to PO_4 in marine particles from the western part of the ETSP have been linked to the development of a heterotrophic population, in contrast to a mix of autotrophic and heterotrophic populations in its eastern part (D. C. Ohnemus et al., 2017). These authors found (1) a peak of acid-volatile sulfides that is used to quantity the monosulfides species (FeS, ZnS, NiS, and CdS) in the first 50 m of the ODZ, and (2) a Cd:AVS (acid-volatile sulfides) abundance of 1:1 or less for the samples lying within the ODZ. However, particulate Cd is expected to be present as either organically bound Cd or CdS in the ODZ, and Cd would be the most susceptible trace metal to precipitate as sulphide based on its stability constant ($\log K_{Cd(HS^-)} = 9.13 \pm 0.02$) for CdS precipitation (D. Guinoiseau et al., 2018). Therefore, the particulate Cd enrichment observed in this ODZ is most likely driven by CdS precipitation rather than only changes in ecological communities.

The role and importance of sulfide precipitates in the biogeochemical cycling of trace metals in oceanic ODZ are still not well constrained. The efficiency in sequestering oceanic Cd into oceanic sediments largely

depends on the extent of CdS oxidation in more oxygenated waters located between the ODZ and the sea floor. It is still unclear, for example, whether CdS remains "stable" under oxic conditions or "slowly" redissolves due to oxidation. The Cd flux to the bottom sediment as CdS particles can be estimated assuming that CdS dissolution follows first-order kinetics. The annual amount of CdS precipitated in the global ocean was recently determined by Bianchi et al. (2018) using their size-resolved particle model (F_{Cd} = 1.4.10^9 molCd/yr). Since the dissolution rate of CdS in seawater (k_s in day^{-1}) is not experimentally known, we considered a range of k_s values based on data from different CdS oxidation experiments and on model parameter optimization reported in the literature (Figure S8). The used k_s values were obtained from 15 and 24 hr dissolution experiments of CdS particles in water (D. M. Di Toro et al., 1996; S. L. Simpson et al., 2000), from thermodynamic calculation of CdS particle dissolution in soil (J. P. Gustafsson, 2013) or by calculations based on analogous ZnS dissolution experiments (A. Voegelin et al., 2011, see Figure S8). The optimized k_s values derived from the Bianchi et al. (2018) model are very high (k_s of 0.15 and 0.33 day^{-1} for the two optimized scenarios, respectively) compared to those from other experimental studies (k_s from 0.01 to 0.094 day^{-1}, D. M. Di Toro et al., 1996; J. P. Gustafsson, 2013; S. L. Simpson et al., 2000; A. Voegelin et al., 2011) and are disregarded here.

The velocity of sinking particles in seawater is highly variable depending on the shape, density, and size of organic particles (McDonnell & Buesseler, 2010). As CdS is expected to precipitate within coarse organic aggregates (>1 mm, D. Bianchi et al., 2018), we applied a range in sinking rates of 70 to 130 m day^{-1}, based on various studies (Fowler & Knauer, 1986; Iversen & Ploug, 2010; McDonnell & Buesseler, 2010). This yields a settling time for CdS particles from the top of the ODZ to the seafloor of 29 to 54 days. Combining settling times and dissolution rates, we estimate the annual CdS flux transferred to seafloor sediments (average depth of 3,800 m) to range from 0.87 to 104 × 10^7 mol/yr (Figure S8). The lower estimate is a nonnegligible sink compared to suboxic [0.03–2.3.10^7 mol/yr, Morford & Emerson, 1999; Y. Rosenthal et al., 1995; A. van Geen et al., 1995) or anoxic (0.09–3.6.10^7 mol/yr; S. H. Little et al., 2015; A. van Geen et al., 1995) sequestration Cd fluxes (Figure S8). The maximum estimate of 104 × 10^7 mol/yr would constitute the main Cd removal mechanism for Cd in the oceans. Obviously, refining the dissolution constant k_s is paramount to better constrain this flux and will be key to establish the oceanic mass balance of Cd at a global scale.

5. Conclusions

Our understanding of the biogeochemical cycling of Cd in the oceans has significantly improved over the past decade by the measurements of Cd isotopes and elemental data on both seawater and particles. In this study, we present new seawater Cd isotope data from the Angola Basin ODZ, one of the major upwelling systems of the world's ocean. We show that at depth, water mass mixing is the main mechanism controlling deepwater Cd isotope signatures as already shown in other oceanic provinces. Near the surface, we modeled Cd isotope fractionation with an open system at steady state buffered by organic ligand complexation. However, in the body of the ODZ, our data show the precipitation of CdS within the microenvironment of sinking biogenic particles. This conclusion, along with previous data, strongly supports the formation of CdS in most ODZ systems worldwide. Based on available particle settling times and CdS dissolution rates estimates, we conclude that CdS precipitation and export acts as a major sink for Cd in the ocean, even if the magnitude of this flux is still very uncertain and worthy of more investigation. In addition to CdS export, the sequestration of Cd within suboxic and anoxic environments and at continental margins are also of importance even if the Cd isotope signatures associated with these fluxes are still unknown. A quantitative sequestration of light Cd has recently been proposed by Janssen et al. (2019) to explain the shift in the particulate δ^{114}Cd toward heavier values at depth. In contrast, it has been argued that Cd enrichment in bottom waters of the Peru Margin is due to oxidation of Cd released from continental margin sediments (R. C. Xie et al., 2019). Future studies will need to constrain the role and importance of margin sediments for the oceanic Cd mass balance, as recently shown to be the case for the marine Zn and Cu cycles (S. H. Little et al., 2016, 2017).

Acknowledgments
The authors deeply thank Christian Schlosser and Jan-Lukas Menzel for sample collection during GA08 and for providing nutrient data. Reimund Jotter and Siegfried Herrmann are thanked for their technical assistance during the acquisition of the chemical and isotope analyses. The authors thank Oliver Baars for providing his unpublished Cd complexation constants on organic ligands determined in the ETSP ODZ. We are grateful to the Editors, Peter Raymond and Ben Twining, reviewer Tim Conway, and an anonymous reviewer for their helpful comments. All the data reported in this study can be found in the supporting information file associated with this manuscript and in the GEOTRACES International Data Assembly Centre (GDAC) (https://www.bodc.ac.uk/geotraces/data/).

References

Abouchami, W., Galer, S. J. G., de Baar, H. J. W., Alderkamp, A. C., Middag, R., Laan, P., et al. (2011). Modulation of the Southern Ocean cadmium isotope signature by ocean circulation and primary productivity. *Earth and Planetary Science Letters*, *305*(1–2), 83–91. https://doi.org/10.1016/j.epsl.2011.02.044

Abouchami, W., Galer, S. J. G., de Baar, H. J. W., Middag, R., Vance, D., Zhao, Y., et al. (2014). Biogeochemical cycling of cadmium isotopes in the Southern Ocean along the Zero Meridian. *Geochimica et Cosmochimica Acta*, *127*, 348–367. https://doi.org/10.1016/j.gca.2013.10.022

Abouchami, W., Galer, S. J. G., Horner, T. J., Rehkämper, M., Wombacher, F., Xue, Z., et al. (2013). A common reference material for cadmium isotope studies—NIST SRM 3108. *Geostandards and Geoanalytical Research*, *37*(1), 5–17. https://doi.org/10.1111/j.1751-908X.2012.00175.x

Anderson, L. A., & Sarmiento, J. L. (1994). Redfield ratios of remineralization determined by nutrient data analysis. *Global Biogeochemical Cycles*, *8*(1), 65–80. https://doi.org/10.1029/93GB03318

Baars, O., Abouchami, W., Galer, S. J. G., Boye, M., & Croot, P. L. (2014). Dissolved cadmium in the Southern Ocean: Distribution, speciation, and relation to phosphate. *Limnology and Oceanography*, *59*(2), 385–399. https://doi.org/10.4319/lo.2014.59.2.0385

Bates, S. L., Hendry, K. R., Pryer, H. V., Kinsley, C. W., Pyle, K. M., Woodward, E. M. S., & Horner, T. J. (2017). Barium isotopes reveal role of ocean circulation on barium cycling in the Atlantic. *Geochimica et Cosmochimica Acta*, *204*, 286–299. https://doi.org/10.1016/j.gca.2017.01.043

Beman, J. M., & Carolan, M. T. (2013). Deoxygenation alters bacterial diversity and community composition in the ocean's largest oxygen minimum zone. *Nature Communications*, *4*, 2705. https://doi.org/10.1038/ncomms3705

Bianchi, D., Weber, T. S., Kiko, R., & Deutsch, C. (2018). Global niche of marine anaerobic metabolisms expanded by particle microenvironments. *Nature Geoscience*, *11*(4), 263–268. https://doi.org/10.1038/s41561-018-0081-0

Bourne, H. L., Bishop, J. K. B., Lam, P. J., & Ohnemus, D. C. (2018). Global spatial and temporal variation of Cd:P in euphotic zone particulates. *Global Biogeochemical Cycles*, *32*(7), 1123–1141. https://doi.org/10.1029/2017GB005842

Boyle, E. A., Sclater, F., & Edmond, J. M. (1976). On the marine geochemistry of cadmium. *Nature*, *263*(5572), 42–44. https://doi.org/10.1038/263042a0

Bruland, K. W. (1980). Oceanographic distributions of cadmium, zinc, nickel, and copper in the North Pacific. *Earth and Planetary Science Letters*, *47*(2), 176–198. https://doi.org/10.1016/0012-821X(80)90035-7

Bruland, K. W. (1992). Complexation of cadmium by natural organic ligands in the central North Pacific. *Limnology and Oceanography*, *37*(5), 1008–1017. https://doi.org/10.4319/lo.1992.37.5.1008

Canfield, D. E., Stewart, F. J., Thamdrup, B., De Brabandere, L., Dalsgaard, T., Delong, E. F., et al. (2010). A cryptic sulfur cycle in oxygen-minimum-zone waters off the Chilean coast. *Science*, *330*(6009), 1375–1378. https://doi.org/10.1126/science.1196889

Carolan, M. T., Smith, J. M., & Beman, J. M. (2015). Transcriptomic evidence for microbial sulfur cycling in the eastern tropical North Pacific oxygen minimum zone. *Frontiers in Microbiology*, *6*, 334. https://doi.org/10.3389/fmicb.2015.00334

Conway, T. M., & John, S. G. (2015a). The cycling of iron, zinc and cadmium in the North East Pacific Ocean—Insights from stable isotopes. *Geochimica et Cosmochimica Acta*, *164*, 262–283. https://doi.org/10.1016/j.gca.2015.05.023

Conway, T. M., & John, S. G. (2015b). Biogeochemical cycling of cadmium isotopes along a high-resolution section through the North Atlantic Ocean. *Geochimica et Cosmochimica Acta*, *148*, 269–283. https://doi.org/10.1016/j.gca.2014.09.032

Cullen, J. T. (2006). On the nonlinear relationship between dissolved cadmium and phosphate in the modern global ocean: Could chronic iron limitation of phytoplankton growth cause the kink? *Limnology and Oceanography*, *51*(3), 1369–1380. https://doi.org/10.4319/lo.2006.51.3.1369

Cullen, J. T., Lane, T. W., Morel, F. M. M., & Sherrell, R. M. (1999). Modulation of cadmium uptake in phytoplankton by seawater CO_2 concentration. *Nature*, *402*(6758), 165–167. https://doi.org/10.1038/46007

de Baar, H. J. W., Saager, P. M., Nolting, R. F., & van der Meer, J. (1994). Cadmium versus phosphate in the world ocean. *Marine Chemistry*, *46*(3), 261–281. https://doi.org/10.1016/0304-4203(94)90082-5

Di Toro, D. M., Mahony, J. D., Hansen, D. J., & Berry, W. J. (1996). A model of the oxidation of iron and cadmium sulfide in sediments. *Environmental Toxicology and Chemistry*, *15*(12), 2168–2186. https://doi.org/10.1002/etc.5620151212

Ellwood, M. J. (2008). Wintertime trace metal (Zn, Cu, Ni, Cd, Pb and Co) and nutrient distributions in the Subantarctic Zone between 40–52°S; 155–160°E. *Marine Chemistry*, *112*(1–2), 107–117. https://doi.org/10.1016/j.marchem.2008.07.008

Fowler, S. W., & Knauer, G. A. (1986). Role of large particles in the transport of elements and organic compounds through the oceanic water column. *Progress in Oceanography*, *16*(3), 147–194. https://doi.org/10.1016/0079-6611(86)90032-7

Fuchs, B. M., Woebken, D., Zubkov, M. V., Burkill, P., & Amann, R. (2005). Molecular identification of picoplankton populationsin contrasting waters of the Arabian Sea. *Aquatic Microbial Ecology*, *39*(2), 145–157. https://doi.org/10.3354/ame039145

Gault-Ringold, M., Adu, T., Stirling, C. H., Frew, R. D., & Hunter, K. A. (2012). Anomalous biogeochemical behavior of cadmium in subantarctic surface waters: Mechanistic constraints from cadmium isotopes. *Earth and Planetary Science Letters*, *341–344*, 94–103.

George, E., Stirling, C. H., Gault-Ringold, M., Ellwood, M. J., & Middag, R. (2019). Marine biogeochemical cycling of cadmium and cadmium isotopes in the extreme nutrient-depleted subtropical gyre of the South West Pacific Ocean. *Earth and Planetary Science Letters*, *514*, 84–95. https://doi.org/10.1016/j.epsl.2019.02.031

Guinoiseau, D., Galer, S. J. G., & Abouchami, W. (2018). Effect of cadmium sulphide precipitation on the partitioning of Cd isotopes: Implications for the oceanic Cd cycle. *Earth and Planetary Science Letters*, *498*, 300–308. https://doi.org/10.1016/j.epsl.2018.06.039

Gustafsson, J. P. (2013). *Soil chemical behaviour of cadmium pigments from paints*. Stockholm: Swedish Chemical Agency.

Horner, T. J., Kinsley, C. W., & Nielsen, S. G. (2015). Barium-isotopic fractionation in seawater mediated by barite cycling and oceanic circulation. *Earth and Planetary Science Letters*, *430*, 511–522. https://doi.org/10.1016/j.epsl.2015.07.027

Iversen, M. H., & Ploug, H. (2010). Ballast minerals and the sinking carbon flux in the ocean: Carbon-specific respiration rates and sinking velocity of marine snow aggregates. *Biogeosciences*, *7*(9), 2613–2624. https://doi.org/10.5194/bg-7-2613-2010

Janssen, D. J., Abouchami, W., Galer, S. J. G., & Cullen, J. T. (2017). Fine-scale spatial and interannual cadmium isotope variability in the subarctic northeast Pacific. *Earth and Planetary Science Letters*, *472*, 241–252. https://doi.org/10.1016/j.epsl.2017.04.048

Janssen, D. J., Abouchami, W., Galer, S. J. G., Purdon, K. B., & Cullen, J. T. (2019). Particulate cadmium stable isotopes in the subarctic northeast Pacific reveal dynamic Cd cycling and a new isotopically light Cd sink. *Earth and Planetary Science Letters*, *515*, 67–78. https://doi.org/10.1016/j.epsl.2019.03.006

Janssen, D. J., Conway, T. M., John, S. G., Christian, J. R., Kramer, D. I., Pedersen, T. F., & Cullen, J. T. (2014). Undocumented water column sink for cadmium in open ocean oxygen-deficient zones. *Proceedings of the National Academy of Sciences*, *111*(19), 6888–6893. https://doi.org/10.1073/pnas.1402388111

John, S. G., & Conway, T. M. (2014). A role for scavenging in the marine biogeochemical cycling of zinc and zinc isotopes. *Earth and Planetary Science Letters*, *394*, 159–167. https://doi.org/10.1016/j.epsl.2014.02.053

John, S. G., Helgoe, J., & Townsend, E. (2017). Biogeochemical cycling of Zn and Cd and their stable isotopes in the Eastern Tropical South Pacific. *Marine Chemistry*, *201*, 256–262.

Karstensen, J., & Tomczak, M. (1998). Age determination of mixed water masses using CFC and oxygen data. *Journal of Geophysical Research*, *103*(C9), 18,599–18,609. https://doi.org/10.1029/98JC00889

Lacan, F., Francois, R., Ji, Y., & Sherrell, R. M. (2006). Cadmium isotopic composition in the ocean. *Geochimica et Cosmochimica Acta*, *70*(20), 5104–5118. https://doi.org/10.1016/j.gca.2006.07.036

Lambelet, M., Rehkämper, M., van de Flierdt, T., Xue, Z., Kreissig, K., Coles, B., et al. (2013). Isotopic analysis of Cd in the mixing zone of Siberian rivers with the Arctic Ocean—New constraints on marine Cd cycling and the isotope composition of riverine Cd. *Earth and Planetary Science Letters*, *361*, 64–73. https://doi.org/10.1016/j.epsl.2012.11.034

Lane, E. S., Semeniuk, D. M., Strzepek, R. F., Cullen, J. T., & Maldonado, M. T. (2009). Effects of iron limitation on intracellular cadmium of cultured phytoplankton: Implications for surface dissolved cadmium to phosphate ratios. *Marine Chemistry*, *115*(3–4), 155–162. https://doi.org/10.1016/j.marchem.2009.07.008

Lass, H. U., Schmidt, M., Mohrholz, V., & Nausch, G. (2000). Hydrographic and current measurements in the area of the Angola–Benguela Front. *Journal of Physical Oceanography*, *30*(10), 2589–2609. https://doi.org/10.1175/1520-0485(2000)030<2589:HACMIT>2.0.CO;2

Little, S. H., Vance, D., Lyons, T. W., & McManus, J. (2015). Controls on trace metal authigenic enrichment in reducing sediments: Insights from modern oxygen-deficient settings. *American Journal of Science*, *315*(2), 77–119. https://doi.org/10.2475/02.2015.01

Little, S. H., Vance, D., McManus, J., & Severmann, S. (2016). Key role of continental margin sediments in the oceanic mass balance of Zn and Zn isotopes. *Geology*, *44*(3), 207–210. https://doi.org/10.1130/G37493.1

Little, S. H., Vance, D., McManus, J., Severmann, S., & Lyons, T. W. (2017). Copper isotope signatures in modern marine sediments. *Geochimica et Cosmochimica Acta*, *212*, 253–273. https://doi.org/10.1016/j.gca.2017.06.019

Mawji, E., Schlitzer, R., Dodas, E. M., Abadie, C., Abouchami, W., Anderson, R. F., et al. (2015). The GEOTRACES Intermediate Data Product 2014. *Marine Chemistry*, *177*, 1–8. https://doi.org/10.1016/j.marchem.2015.04.005

McDonnell, A. M. P., & Buesseler, K. O. (2010). Variability in the average sinking velocity of marine particles. *Limnology and Oceanography*, *55*(5), 2085–2096. https://doi.org/10.4319/lo.2010.55.5.2085

Middag, R., van Heuven, S. M. A. C., Bruland, K. W., & de Baar, H. J. W. (2018). The relationship between cadmium and phosphate in the Atlantic Ocean unravelled. *Earth and Planetary Science Letters*, *492*, 79–88. https://doi.org/10.1016/j.epsl.2018.03.046

Morel, F. M. M. (2008). The co-evolution of phytoplankton and trace element cycles in the oceans. *Geobiology*, *6*(3), 318–324. https://doi.org/10.1111/j.1472-4669.2008.00144.x

Morford, J. L., & Emerson, S. (1999). The geochemistry of redox sensitive trace metals in sediments. *Geochimica et Cosmochimica Acta*, *63*(11-12), 1735–1750. https://doi.org/10.1016/S0016-7037(99)00126-X

Ohnemus, D. C., Rauschenberg, S., Cutter, G. A., Fitzsimmons, J. N., Sherrell, R. M., & Twining, B. S. (2017). Elevated trace metal content of prokaryotic communities associated with marine oxygen deficient zones. *Limnology and Oceanography*, *62*(1), 3–25. https://doi.org/10.1002/lno.10363

Quay, P., Cullen, J., Landing, W., & Morton, P. (2015). Processes controlling the distributions of Cd and PO4 in the ocean. *Global Biogeochemical Cycles*, *29*, 830–841. https://doi.org/10.1002/2014GB004998

Ripperger, S., Rehkämper, M., Porcelli, D., & Halliday, A. N. (2007). Cadmium isotope fractionation in seawater—A signature of biological activity. *Earth and Planetary Science Letters*, *261*(3–4), 670–684. https://doi.org/10.1016/j.epsl.2007.07.034

Rosenthal, Y., Boyle, E. A., Labeyrie, L., & Oppo, D. (1995). Glacial enrichments of authigenic Cd and U in subantarctic sediments: A climatic control on the elements' oceanic budget? *Paleoceanography*, *10*(3), 395–413. https://doi.org/10.1029/95PA00310

Roshan, S., & Wu, J. (2015). Cadmium regeneration within the North Atlantic. *Global Biogeochemical Cycles*, *29*, 2082–2094. https://doi.org/10.1002/2015GB005215

Roshan, S., Wu, J., & DeVries, T. (2017). Controls on the cadmium-phosphate relationship in the tropical South Pacific. *Global Biogeochemical Cycles*, *31*, 1516–1527. https://doi.org/10.1002/2016GB005556

Schlitzer, R. (2018), Ocean data view, edited.

Schmitt, A.-D., Galer, S. J. G., & Abouchami, W. (2009). High-precision cadmium stable isotope measurements by double spike thermal ionisation mass spectrometry. *Journal of Analytical Atomic Spectrometry*, *24*(8), 1079–1088. https://doi.org/10.1039/b821576f

Sieber, M., Conway, T. M., de Souza, G. F., Obata, H., Takano, S., Sohrin, Y., & Vance, D. (2018). Physical and biogeochemical controls on the distribution of dissolved cadmium and its isotopes in the Southwest Pacific Ocean. *Chemical Geology*, *511*, 494–509. https://doi.org/10.1016/j.chemgeo.2018.07.021

Simpson, S. L., Apte, S. C., & Batley, G. E. (2000). Effect of short-term resuspension events on the oxidation of cadmium, lead, and zinc sulfide phases in anoxic estuarine sediments. *Environmental Science & Technology*, *34*(21), 4533–4537. https://doi.org/10.1021/es991440x

Stramma, L., & England, M. (1999). On the water masses and mean circulation of the South Atlantic Ocean. *Journal of Geophysical Research*, *104*(C9), 20,863–20,883. https://doi.org/10.1029/1999JC900139

Suga, T., & Talley, L. D. (1995). Antarctic Intermediate Water circulation in the tropical and subtropical South Atlantic. *Journal of Geophysical Research*, *100*(C7), 13,441–13,453. https://doi.org/10.1029/95JC00858

Van Bennekom, A. J., & Berger, G. W. (1984). Hydrography and silica budget of the Angola Basin. *Netherlands Journal of Sea Research*, *17*(2-4), 149–200. https://doi.org/10.1016/0077-7579(84)90047-4

van Geen, A., McCorkle, D. C., & Klinkhammer, G. P. (1995). Sensitivity of the phosphate-cadmium-carbon isotope relation in the ocean to cadmium removal by suboxic sediments. *Paleoceanography*, *10*(2), 159–169. https://doi.org/10.1029/94PA03352

Voegelin, A., Jacquat, O., Pfister, S., Barmettler, K., Scheinost, A. C., & Kretzschmar, R. (2011). Time-dependent changes of zinc speciation in four soils contaminated with zincite or sphalerite. *Environmental Science & Technology*, *45*(1), 255–261. https://doi.org/10.1021/es101189d

Waeles, M., Maguer, J.-F., Baurand, F., & Riso, R. D. (2013). Off Congo waters (Angola Basin, Atlantic Ocean): A hot spot for cadmium-phosphate fractionation. *Limnology and Oceanography*, *58*(4), 1481–1490. https://doi.org/10.4319/lo.2013.58.4.1481

Wu, J., & Roshan, S. (2015). Cadmium in the North Atlantic: Implication for global cadmium–phosphorus relationship. *Deep Sea Research Part II: Topical Studies in Oceanography*, *116*, 226–239. https://doi.org/10.1016/j.dsr2.2014.11.007

Xie, R. C., Galer, S. J. G., Abouchami, W., & Frank, M. (2018). Limited impact of eolian and riverine sources on the biogeochemical cycling of Cd in the tropical Atlantic. *Chemical Geology*, *511*, 371–379.

Xie, R. C., Galer, S. J. G., Abouchami, W., Rijkenberg, M. J. A., de Baar, H. J. W., De Jong, J., & Andreae, M. O. (2017). Non-Rayleigh control of upper-ocean Cd isotope fractionation in the western South Atlantic. *Earth and Planetary Science Letters*, *471*, 94–103. https://doi.org/10.1016/j.epsl.2017.04.024

Xie, R. C., Galer, S. J. G., Abouchami, W., Rijkenberg, M. J. A., De Jong, J., de Baar, H. J. W., & Andreae, M. O. (2015). The cadmium–phosphate relationship in the western South Atlantic—The importance of mode and intermediate waters on the global systematics. *Marine Chemistry*, *177*(Part 1), 110–123. https://doi.org/10.1016/j.marchem.2015.06.011

Xie, R. C., Rehkämper, M., Grasse, P., van de Flierdt, T., Frank, M., & Xue, Z. (2019). Isotopic evidence for complex biogeochemical cycling of Cd in the eastern tropical South Pacific. *Earth and Planetary Science Letters*, *512*, 134–146. https://doi.org/10.1016/j.epsl.2019.02.001

Xue, Z., Rehkämper, M., Horner, T. J., Abouchami, W., Middag, R., van de Flierd, T., & de Baar, H. J. W. (2013). Cadmium isotope variations in the Southern Ocean. *Earth and Planetary Science Letters*, *382*, 161–172. https://doi.org/10.1016/j.epsl.2013.09.014

Yang, J., Li, Y., Liu, S., Tian, H., Chen, C., Liu, J., & Shi, Y. (2015). Theoretical calculations of Cd isotope fractionation in hydrothermal fluids. *Chemical Geology*, *391*, 74–82. https://doi.org/10.1016/j.chemgeo.2014.10.029

Yang, S.-C., Lee, D.-C., & Ho, T.-Y. (2015). Cd isotopic composition in the suspended and sinking particles of the surface water of the South China Sea: The effects of biotic activities. *Earth and Planetary Science Letters*, *428*, 63–72. https://doi.org/10.1016/j.epsl.2015.07.025

Yang, S.-C., Zhang, J., Sohrin, Y., & Ho, T.-Y. (2018). Cadmium cycling in the water column of the Kuroshio-Oyashio Extension region: Insights from dissolved and particulate isotopic composition. *Geochimica et Cosmochimica Acta*, *233*, 66–80. https://doi.org/10.1016/j.gca.2018.05.001

Yeats, P. A., Westerlund, S., & Flegal, A. R. (1995). Cadmium, copper and nickel distributions at four stations in the eastern central and south Atlantic. *Marine Chemistry*, *49*(4), 283–293. https://doi.org/10.1016/0304-4203(95)00018-M

References From the Supporting Information

Barrett, K. A., & McBride, M. B. (2007). Dissolution of zinc-cadmium sulfide solid solutions in aerated aqueous suspension. *Soil Science Society of America Journal*, *71*(2), 322–328. https://doi.org/10.2136/sssaj2006.0124

Ellwood, M. J. (2004). Zinc and cadmium speciation in subantarctic waters east of New Zealand. *Marine Chemistry*, *87*(1-2), 37–58. https://doi.org/10.1016/j.marchem.2004.01.005

Gustafsson, J. P. (2017). Visual MINTEQ, Ver.3.1, edited by https://vminteq.lwr.kth.se/

Horner, T. J., Rickaby, R. E. M., & Henderson, G. M. (2011). Isotopic fractionation of cadmium into calcite. *Earth and Planetary Science Letters*, *312*(1–2), 243–253. https://doi.org/10.1016/j.epsl.2011.10.004

Wasylenki, L. E., Swihart, J. W., & Romaniello, S. J. (2014). Cadmium isotope fractionation during adsorption to Mn oxyhydroxide at low and high ionic strength. *Geochimica et Cosmochimica Acta*, *140*, 212–226. https://doi.org/10.1016/j.gca.2014.05.007